Analytical Model of a "Split-Coil" for Implementation of novel Type of Receive Coil in Magnetic Resonance Imaging

Enrico Pannicke[1,3], Oliver Speck[2,3], Ralf Vick[2]

Abstract— In this work implementing MR receive coils from overlapping traces is investigated. Such a configuration is known from Microstrip transmission line (MTL) coils, which are basically used in Magnetic resonance - ultra high field (MR-UHF) imaging as TX-RX volume coils. Applications at lower field strengths are less common, because the required electrical length is more difficult to satisfy as the frequency decreases. Overlapping traces are already known for lower field strengths like $1.5\,\mathrm{T}$ or $3\,\mathrm{T}$. Such configurations provide the ability of reducing the number of lumped on such a coil becoming more flexible. To investigate such a flexible coil the overlap is extended to much larger degree and it will be shown that this setup can be modeled as classical transmission line. An analytical model is developed and verified with simulations providing accurate calculations of the input impedance. This allows a reliable derivation of its parameters, which simplifies implementation of such coils.

I. INTRODUCTION

In this work, the possibility of building conductor loops for MR receiving coils using overlapping copper traces is investigated. Such a configuration is known from Microstrip transmission line (MTL) coils, which are basically used in Magnetic resonance - ultra high field (MR-UHF) imaging as TX-RX volume coils. They differ significantly in geometry from circular loops and consist of straight line elements, tuned to an electrical length of $\lambda/4$ [1] [2].

Their ease of manufacture, good performance and reasonable coverage with a comparably small number of elements recommends it as a plausible alternative. Applications at lower field strengths are less common, because the required electrical length is more difficult to satisfy as the frequency decreases. In this work, the possibility of building MR receive coils based on overlapping traces is investigated. Such configurations are already known from other studies [3] for lower field strengths like $1.5\,\mathrm{T}$ or $3\,\mathrm{T}$ to create flexible MR coils.

In contrast to former studies the overlap is extended to much larger degree and it will be shown that this setup can be modeled as classical transmission line. Based on this insight an analytical model could be developed and verified with simulations providing accurate calculations of the input impedance. This allows a reliable derivation of its parameters and a efficient tuning an matching procedure.

[1]Enrico Pannicke and Ralf Vick are with the Chair of Electromagnetic Compatibility, Otto-von-Guericke University Magdeburg, Germany `enrico.pannicke@ovgu.de`

[2] Oliver Speck is with the Chair of Biomedical Magnetic Resonance, Otto-von-Guericke University Magdeburg, Germany

[3] Enrico Pannicke and Oliver Speck are involved with Research Campus *STIMULATE*, Otto von Guericke University, Magdeburg, SA 39106, Germany
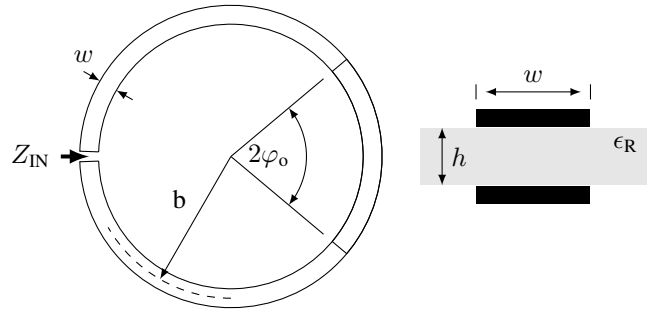
Fig. 1. Geometrical setup of the proposed "SplitCoil". The in plane shift of the traces is only for better visualization.

II. METHODS

The so called "Split-Coil" is shown in Fig. 1 and consists of two circular arcs of copper traces, with loop radius b and trace width w overlapped by a degree of $2\varphi_{\mathrm{o}}$. Both traces are separated by a dielectric, with relative permittivity ϵ_{R} and thickness h. The corresponding input impedance as a function of the normalized electrical length kb for different degrees of overlapping is demonstrated in Fig. 2. The parameter kb normalizes the freespace wavenumber k with the loop radius b.

Especially for low frequencies, the capacitive impedance $Z_{\mathrm{IN}} \approx 1/j\omega C_{\mathrm{G}}$ of the "Split-Coil" differs fundamentally from the inductive curve of a normal conductor loop $Z_{\mathrm{IN}} \approx j\omega L_{\mathrm{S}}$. Fig. 2 demonstrates clearly that the capacitance C_{G} is influenced by the degree of overlap. In principle, the overlapping conductor paths can be modeled as a concentrated capacitor. The drawback of this approach is that any propagation effects along the line are neglected, thus representing a quasi-static approximation. In the following, it is investigated whether a lumped approach is sufficient to adequately model the present arrangement or whether a much more complex approach must be used. Therefore two models are developed and compared with each other regarding their accuracy and predictability.

A. 1. Model: Concentrated Capacitor

A "quasi-static" simplification of the "Split-Coil" is shown in Fig. 3. The overlapping traces form a lumped capacitor, which is located opposite to the feeding port. This capacitance C_{P} can be calculated using the overlapping area A, the dielectric properties of the substrate ϵ_{R}, and the substrate
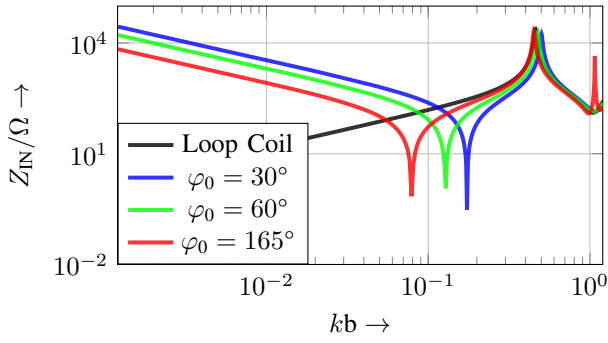
Fig. 2. Input impedance Z_{IN} of the proposed "Split-Coil" for several degrees of overlap φ_{o} ($w = 5\,\text{mm}$, $b = 57.5\,\text{mm}$, $d = 1\,\text{mm}$, $\epsilon_{\text{R}} = 1$) in comparison to a normal loop without overlap.

Fig. 3. Simplified model by replacing the overlapping traces with a lumped capacitor C_{P}.

height h:

$$C_{\text{P}} = \frac{A \cdot \epsilon_0 \cdot \epsilon_{\text{R}}}{h}$$

Increasing the overlap thus leads to an increase in capacitance by enlarging the cross-sectional area, which corresponds well with the course of impedance in the low frequency region. The cross-sectional area of the capacitor is given by the degree of overlap (see Fig. 3) and C_{P} is calculated by

$$C_{\text{P}} = \frac{2 \cdot \varphi_0 \cdot b \cdot w \cdot \epsilon_0 \cdot \epsilon_{\text{R}}}{h} \tag{1}$$

Concentrating the distributed capacitance into one lumped element leads to a circular loop without overlap. As shown in Fig. 3 inserting a lumped capacitance in the mid of the former overlap, the circular loop is becoming a two-port network, which is given by:

$$[\mathbf{Y}]\,(\varphi_1) = \begin{bmatrix} Y_0 & Y_1 \\ Y_1 & Y_0 \end{bmatrix} \tag{2}$$

The parameters Y_0 and Y_1 are calculated by [4]

$$Y_0 = Y_{\text{IN}}\,(a, b) \tag{3}$$

$$Y_{\text{P}} = Y_{\text{IN}}\,(a, b) \cdot \frac{I_1}{I_0} \tag{4}$$

, where the current I_1 is located at the position $\varphi_1 = \pi$ along the circumference of the loop. The input admittance $Y_{\text{IN}}\,(a, b)$ and current $I_{0/1}$ are calculated according to [5], with the equivalent wire radius $a = w/4$ [6].

B. 2. Model: Transmission-Line

The "non static" approximation considers the overlapping traces as symmetric transmission line, which is connected at $\varphi_1 = \pi - \varphi_0$ and $\varphi_2 = \pi + \varphi_0$ to the circular loop. Inserting the corresponding ports on the loop gives at three-port matrix (See Fig. 4 **A**), which is given by:

$$[\mathbf{Y}] = \begin{bmatrix} Y_0 & Y_1 & Y_2 \\ Y_2 & Y_0 & Y_1 \\ Y_1 & Y_2 & Y_0 \end{bmatrix}. \tag{5}$$

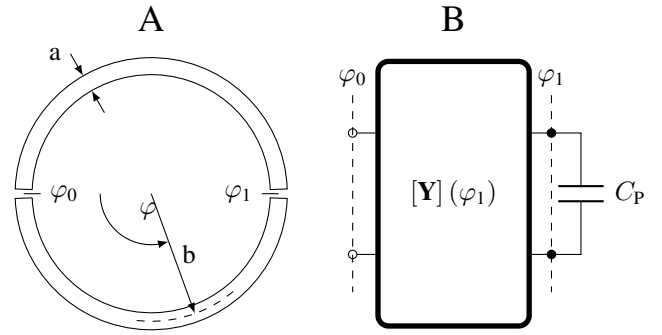Considering the reference impedance Z_{ref}, the addmittance matrix is transformed into a S-parameter representation

$[\mathbf{Y}] \to [\mathbf{S}]$.

The transmission line is inserted between port φ_1 and φ_2 and taking into account that the orientation of the ports is given by φ, we obtain the interconnection of the three-port and two-port shown in Fig. 4 **B**. To account for the fringe fields of the open stubs at the ends of the traces, additional capacitors C_{F} are modeled at the connecting ports.

The S-parameter matrix of the transmission line is calculated by

$$[\mathbf{S}_{\text{MTL}}] = \begin{bmatrix} \dfrac{r \cdot (1 - p^2)}{1 - r^2 \cdot p^2} & \dfrac{p \cdot (1 - r^2)}{1 - r^2 \cdot p^2} \\ \dfrac{p \cdot (1 - r^2)}{1 - r^2 \cdot p^2} & \dfrac{r \cdot (1 - p^2)}{1 - r^2 \cdot p^2} \end{bmatrix} \tag{6}$$

$$r = \frac{Z_0^{\text{DM}} - Z_{\text{ref}}}{Z_0^{\text{DM}} + Z_{\text{ref}}} \tag{7}$$

$$p = \text{e}^{-j\omega(l_{\text{MTL}}/v_{\text{MTL}})} \tag{8}$$

, where Z_0^{DM} is its characteristic impedance, l its geometrical length, v_{MTL} its propagation velocity and Z_{ref} the reference impedance of both ports.

The characteristic impedance of the symmetric transmission
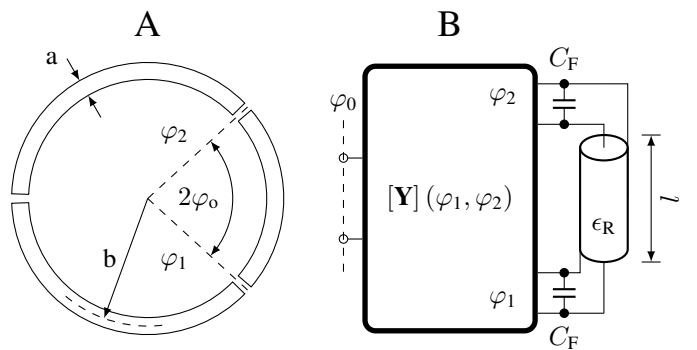

Fig. 4. Second model of the "Split-Coil", which replaces the overlapping traces by a transmission line.

line can be calculated from the characteristic impedance of an unsymmetrical microstrip-line Z_0^{CM}. This is done by introducing a symmetry plane between both traces, which is demonstrated in Fig. 5. The mirroring at this plane allows
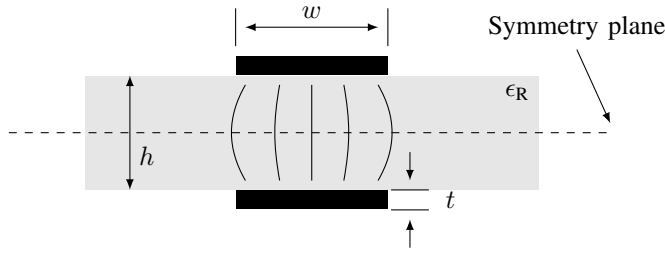
Fig. 5. Conductors within the overlap area. The symmetry plane of the arrangement allows the calculation of the characteristic impedance based on an unbalanced microstrip line.
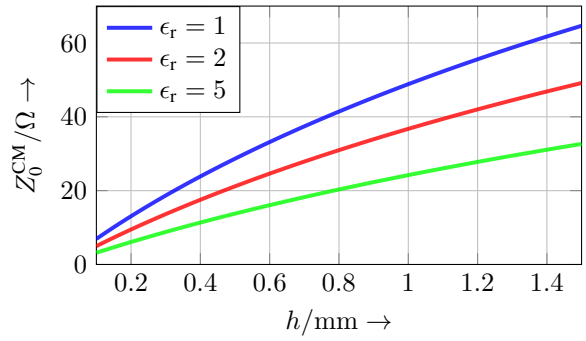

Fig. 6. Characteristic impedance of a microstrip line as a function of spacing between the traces h ($w = 5\,\text{mm}$). for several relative permittivities ϵ_r.

the representation of the symmetric transmission line as a parallel connection of two unsymmetrical transmission lines lines in particular microstrip lines. This leads to

$$Z_0^{\text{DM}} = \frac{Z_0^{\text{CM}}}{2}. \tag{9}$$

, where Z_0^{CM} is calculated by [7]

$$Z_0^{\text{CM}} = \frac{Z_{\text{F0}}/\epsilon_{\text{r,eff}}}{\frac{w_{\text{eff}}}{h_{\text{MTL}}} + 1.393 + \frac{2}{3}\ln\left(\frac{w_{\text{eff}}}{h_{\text{MTL}}} + 1.444\right)}. \tag{10}$$

The effective trace width w_{eff} and effective permittivity $\epsilon_{\text{r,eff}}$ are reduced values of the corresponding parameter, due to the layered dielectric and Z_{F0} is the free space wave impedance. For the proper calculation of Z_0^{CM} the height of unsymmetrical transmission line h_{MTL} is given by

$$h_{\text{MTL}} = \frac{h}{2}. \tag{11}$$

As the effective height h_{MTL} is reduced it seems reasonable that $w/d > 1$ is always satisfied. The effective trace width w_{eff} and permittivity $\epsilon_{\text{r,eff}}$ are calculated by

$$w_{\text{eff}} = h_{\text{MTL}} \cdot \left(\frac{w}{h_{\text{MTL}}} + \frac{5 \cdot t}{4\pi h_{\text{MTL}}} \cdot \left(1 + \ln\left(\frac{2h}{t}\right)\right)\right) \tag{12}$$

$$\epsilon_{\text{r,eff}} = \frac{\epsilon_\text{r} + 1}{2} + \frac{\epsilon_\text{r} - 1}{2} \cdot \frac{1}{\sqrt{1 + 12h_{\text{MTL}}/w}}$$
$$- \frac{\epsilon_\text{r} - 1}{4.6} \cdot \frac{t/w}{\sqrt{w/h_{\text{MTL}}}} \tag{13}$$

Fig. 6 demonstrates the dependence of the characteristic impedance of a microstrip line on the thickness and permittivity of the substrate.
 The length of the microstrip line is calculated according to the overlap

$$l_{\text{MTL}} = 2 \cdot \varphi \cdot \text{b}, \tag{14}$$

and the velocity is reduced by $\epsilon_{\text{r,eff}}$:

$$v_{\text{MTL}} = \frac{1}{\sqrt{\epsilon_0 \cdot \epsilon_{\text{r,eff}} \cdot \mu_0}}. \tag{15}$$

The input impedance Z_{IN} is acquired by terminating $[\textbf{S}]$ with $[\textbf{S}_{\text{MTL}}]$ as shown in Fig. 4.

C. Calibration of parameters

As both models are based on prior calculations of the input admittance $Y(a, b, \epsilon_\text{R})$ of a conventional printed circular loop, its effective relative permittivity $\epsilon_{\text{R,eff}}$ has to be determined [8]. For the second model, the determination of the capacitor C_F is also required. For each configuration, two reference simulations are performed to determine the respective parameters. These included a short- and open-circuit "Split-Coil". The latter configuration is achieved by an overlap angle of $\varphi_\text{o} = 0°$.
The simulation of the short-circuit "Split-Coil" is used to calibrate the effective permittivity $\epsilon_{\text{R,eff}}$ by fitting $Y(a, b, \epsilon_\text{R})$ to the simulation results by the means of "Differential Evolution" (DE) optimization [9].
For the fringe capacitance C_F the open circuit simulation is used. According to Fig. 4 (**A**) the open circuit is achieved by $\varphi \to 0$ and removal of the transmission line, which puts the fringe capacitance's C_F on both ports into series. Therefore the equivalent Fig. 4 (**A**) is transferred into Fig. 3 (**A**) with $C_\text{P} = C_\text{F}/2$. With this insight the fringe capacitance can be determined by fitting the representation in Fig. 3 **B** to the results of the simulation as demonstrated in Fig. 7.
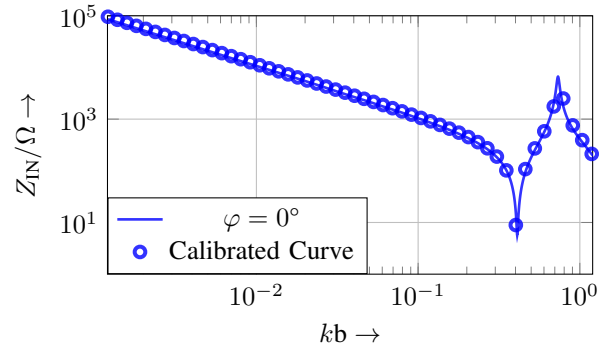

Fig. 7. Determination of C_F by DE-optimization to an open "Split-Coil" ($\varphi = 0°$).

D. Comparison of both models

To evaluate both models, they are compared with simulated data in terms of their accuracy and the predictability

of the necessary parameters. The parameters of the simulated "Split-Coil" are summarized in Tab. I. An openSource FDTD-Solver (openEMS, [10]) was used for the EM-Simulations of an unloaded and loaded "Split-Coil". The latter includes a phantom ($\epsilon_R = 80$, $\kappa = 0.46\,\mathrm{S\,m^{-1}}$) in a distance $d = 5\,\mathrm{mm}$ below the "Split-Coil".

To demonstrate the feasibility of the approach tuning and matching of the "Split-Coil" was conducted based on the best fitting model and validated by EM-simulations. The parameter for these "Split-Coil" are found in Tab. I.

Parameter	Value	Parameter	Value
Model validation			
b	5.75 cm	h	1 mm
a	5 mm	ϵ_R	1...5
Matching & Tuning			
b	6.75 cm	h	0.1 mm
a	2.5 mm	ϵ_R	2.5

TABLE I

PARAMETERS OF THE "SPLIT-COIL" FOR DEMONSTRATING THE

PERFORMANCE OF BOTH MODELS.

III. RESULTS

The result for the first modeling method can be seen in Fig. 8. The curve tends to be more correct for higher frequencies than for the low frequency range. Especially around the first minimum large discrepancies are apparent between simulation and model, which are increased with enlarged degree of overlap.

Additional resonance became apparent in the input impedance for increased electrical lengths of the overlap, which is shown in Fig. 9. These are not correctly reproduced by the lumped element model. Thus the model produces discrepancies in the lower and upper frequency range.

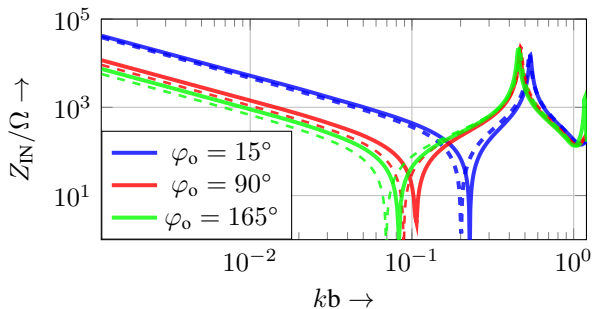In Fig. 10 the results for the second model in comparison to

Fig. 8. Simulated (line) and calculated (dashed) input impedance Z_{IN} of the "Split-Coil" according to the first model (lumped element).

numerical data is shown. In contrast to the previous results, decisive features can be reproduced over the entire frequency range with the second model (i.e. see Fig. 9). The parameters determined by the outlined calibration procedure are summarized in Tab. III. It should be noted that the calibrated values
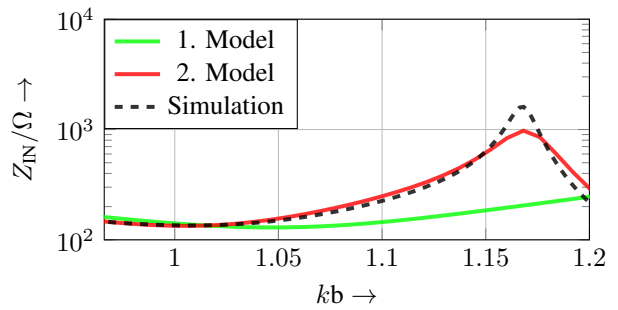
Fig. 9. Numerical (line) and calculated (marks) results of input impedance Z_{IN} of the "Split-Coil" in the high frequency range.

for $b = 57.5\,\mathrm{mm}$ could be used for further setups of different loop radii. Obviously the fringe capacitance C_F is scaled by the relative permittivity ϵ_R.

The corresponding results for $\epsilon_R = 5$ is shown in Fig. 11. As before, regardless of the overlap, the calculated impedance demonstrates a good agreement with numerical results. This is also true if the "Split-Coil" is loaded with a phantom, which is demonstrated in Fig. 12.

The results for the matching and tuning of a larger "Split-

b	5.75 cm	h	1 mm	w	1 mm
$\epsilon_R = 1$		$\epsilon_{R,eff}$	1	C_F	0.36 pF
$\epsilon_R = 5$		$\epsilon_{R,eff}$	1.3	C_F	1.8 pF

Coil" (b = 6.75 cm, $h = 0.1\,\mathrm{mm}$, a = 2.5 mm , $\epsilon_R = 2.5$) are demonstrated in Fig. 13. A required overlap of $\varphi_o = 21°$ could be extracted from the model for proper tuning ($\mathrm{Re}\{Z_{IN}\} = 50\,\Omega$). The matching was achieved by capacitive compensation with extraction of parameters from the proposed model as well.
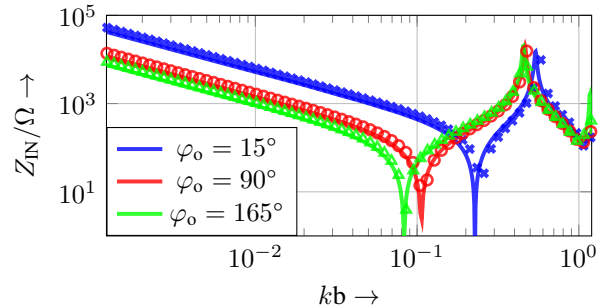
Fig. 10. Simulated input impedance Z_{IN} (line) for different overlap angles φ and $\epsilon_R = 1$ compared to the results of the second model (marks).

IV. DISCUSSION

Two models for the proposed "Split-Coil" were demonstrated and evaluated. The first model inherits the advantage of its simplicity, since $[\mathbf{Y}]$ has to be calculated only once no matter which overlap is required.

A more detailed comparison for an overlap of $\varphi = 30°$ is shown in Fig. 14. Although the calculated capacitance $C_P = 5.33\,\mathrm{pF}$ corresponds well to the impedance of the total capacitance Z_C in the low frequency range, the resonance
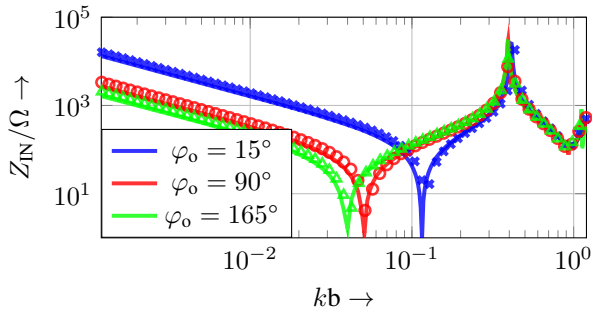
Fig. 11. Simulated input impedance Z_{IN} (line) for different overlap angles φ and $\epsilon_R = 5$ compared to the results of the second model (marks).
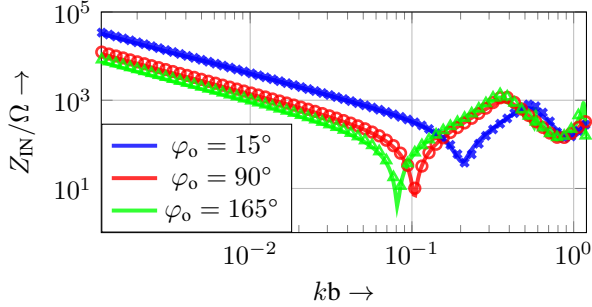

Fig. 12. Simulated input impedance Z_{IN} (line) of a loaded "Split-Coil" (Phantom: $\epsilon_R = 80$, $\kappa = 0.46\,\mathrm{S\,m^{-1}}$) for different overlap angles φ and air substrate ($\epsilon_R = 1$) compared to the results of the second model (marks).

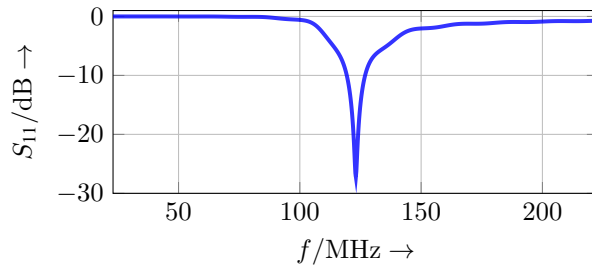Fig. 13. Simulated reflection coefficient S_{11} of a "Split-Coil" with a overlap of $\varphi_o = 21°$.

frequency of the first minimum f_0 is not predicted properly by the first model.

The increasing deviations for larger overlaps indicate that the propagation effects along them are not negligible, which is clearly evident for higher frequencies where additional resonances appear in the input impedance curve. These resonance are not reproduce by lumped capacitors, which is clearly demonstrated in Fig. 9.

The second model provides superior agreement with numerical results over the whole frequency range. Most parameters can be predicted by already existing equations for a microstrip-line. The effective relative permittivity of a printed loop on a substrate $\epsilon_{R,eff}$ and the fringe capacitance C_F have to be calibrated. A proper strategy for this could be presented, but still represents one of the most important drawbacks of the method as it still relies on additional simulations or measurements. Preliminary results seems to indicate that the fringe capacitance C_F is independent on the loop radius b, which simplifies the procedure. This seems reasonable as
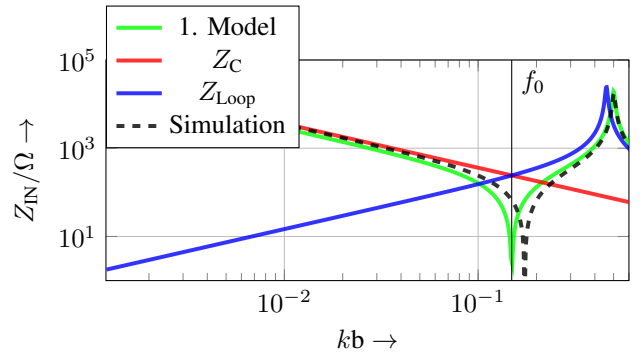

Fig. 14. Input impedance Z_{IN} of the "Split-Coil" for a degree of overlap $\varphi = 30°$ calculated by the lumped element approach compared to a reference simulation.

the capacitance between the stub and opposing trace should depend on h, ϵ_R and w, which is subject to future studies.

For use as a receive coil during MR imaging, the coils need to be matched to the a certain reference impedance (typically $Z_{ref} = 50\,\Omega$) to preserve the intrinsic SNR as much as possible [11]. As the input impedance is adjustable by geometrical modifications of the "Split-Coil" the demonstrated models serve as important mean to optimize its parameters with respect to a specific reference impedance. A first prove of concept of its feasibility was demonstrated in these work. Further studies will concentrate on the aspect of calibration, as the need of preliminary simulations is one of the major obstacles for an efficient workflow.

ACKNOWLEDGMENT

REFERENCES

[1] X. Zhang, K. Ugurbil, and W. Chen, "Microstrip rf surface coil design for extremely high-field mri and spectroscopy," *Magnetic Resonance in Medicine*, vol. 46, no. 3, pp. 443–450, 2001.

[2] T. Wichmann, D. Gareis, M. Griswold, T. Neuberger, S. Wright, C. Faber, A. Webb, and P. Jakob, "A four channel transmit receive microstrip array for 17.6 t," *Proc 12th ISMRM*, 01 2004.

[3] J. R. Corea, A. M. Flynn, B. Lechêne, G. Scott, G. D. Reed, P. J. Shin, M. Lustig, and A. C. Arias, "Screen-printed flexible mri receive coils," *Nature communications*, vol. 7, no. 1, pp. 1–7, 2016.

[4] R. F. Harrington and J. Mautz, "Electromagnetic behaviour of circular wire loops with arbitrary excitation and loading," *Proceedings of the Institution of Electrical Engineers*, vol. 115, no. 1, pp. 68–77, 1968.

[5] T. T. Wu, "Theory of the thin circular loop antenna," *Journal of Mathematical Physics*, vol. 3, no. 6, pp. 1301–1304, 1962.

[6] H. A. N. Hejase, "Analysis of a printed wire loop antenna," *IEEE Transactions on Microwave Theory and Techniques*, vol. 42, no. 2, pp. 227–233, 1994.

[7] H. A. Wheeler, "Transmission-line properties of parallel strips separated by a dielectric sheet," *IEEE Transactions on Microwave Theory and Techniques*, vol. 13, no. 2, pp. 172–185, 1965.

[8] R. King, C. Harrison, and D. Tingley, "The admittance of bare circular loop antennas in a dissipative medium," *IEEE Transactions on Antennas and Propagation*, vol. 12, no. 4, pp. 434–438, 1964.

[9] U. K. Chakraborty, *Advances in differential evolution*, vol. 143. Springer, 2008.

[10] T. Liebig, "openems - open electromagnetic field solver."

[11] J. Mispelter, M. Lupu, and A. Briguet, *NMR Probeheads for Biophysical and Biomedical Experiments: Theoretical Principles & Practical Guidelines*. Imperial College Press, 2006.